SCIENTIFIC REPORTS

OPEN

SUBJECT AREAS:
IMAGING TECHNIQUES AND AGENTS
NANOPARTICLES

Received
28 April 2014

Accepted
17 June 2014

Published
4 July 2014

Correspondence and requests for materials should be addressed to H.-C.C. (hchang@gate.sinica.edu.tw)

* These authors contributed equally to this work.

Wide-field imaging and flow cytometric analysis of cancer cells in blood by fluorescent nanodiamond labeling and time gating

Yuen Yung Hui[1]*, Long-Jyun Su[1,2]*, Oliver Yenjyh Chen[1], Yit-Tsong Chen[2], Tzu-Ming Liu[3] & Huan-Cheng Chang[1]

[1]Institute of Atomic and Molecular Sciences, Academia Sinica, Taipei 106, Taiwan, [2]Department of Chemistry, National Taiwan University, Taipei 106, Taiwan, [3]Institute of Biomedical Engineering, National Taiwan University, Taipei 100, Taiwan.

Nanodiamonds containing high density ensembles of negatively charged nitrogen-vacancy (NV^-) centers are promising fluorescent biomarkers due to their excellent photostability and biocompatibility. The NV^- centers in the particles have a fluorescence lifetime of up to 20 ns, which distinctly differs from those (<10 ns) of cell and tissue autofluorescence, making it possible to achieve background-free detection *in vivo* by time gating. Here, we demonstrate the feasibility of using fluorescent nanodiamonds (FNDs) as optical labels for wide-field time-gated fluorescence imaging and flow cytometric analysis of cancer cells with a nanosecond intensified charge-coupled device (ICCD) as the detector. The combined technique has allowed us to acquire fluorescence images of FND-labeled HeLa cells in whole blood covered with a chicken breast of ~0.1-mm thickness at the single cell level, and to detect individual FND-labeled HeLa cells in blood flowing through a microfluidic device at a frame rate of 23 Hz, as well as to locate and trace FND-labeled lung cancer cells in the blood vessels of a mouse ear. It opens a new window for real-time imaging and tracking of transplanted cells (such as stem cells) *in vivo*.

Long-term imaging and tracking of cells *in vivo* is a highly valuable technique in life sciences[1]. It demands a fluorescent marker far more photostable than organic dyes and far less toxic than quantum dots for labeling[2]. Fluorescent nanodiamond (FND) has recently emerged as a promising bioimaging agent because this carbon-based nanomaterial is inherently non-toxic, highly biocompatible, readily conjugated with biomolecules, and can be easily taken up by cells[3]. Moreover, it can emit multicolor fluorescence from crystal defects[4]. The negatively charged nitrogen-vacancy center, NV^-, is of particular interest in this category since its fluorescence emission lies in the near-infrared window of bioimaging. The centers are photostable even when they are encased in diamond crystallites of ~5 nm in diameter[5]. All these traits make FND one of the best candidates for high-resolution imaging and long-term tracking in complex biological environments.

A unique feature of the NV^- center in FND is that its far-red fluorescence has a long-lived lifetime of $\tau >$ 10 ns[6,7], which is significantly longer than those of the endogenous fluorophores in cells and tissues[8]. Hence, time-gating techniques can be exploited to separate the FND emission from strong cell/tissue autofluorescence to enhance image contrast[9,10]. This opens up a new opportunity to achieve wide-field background-free detection of FND-labeled cells *in vivo*. Igarashi *et al.*[11] have recently developed an approach to improve the image contrast of FNDs in living organisms by taking advantage of the spin property of the NV^- center[12]. The authors acquired wide-field fluorescence images with and without microwave radiation on resonance with the crystal-field splitting (2.87 GHz) of the ground-state spins. As a result that the alternative microwave irradiation modulated only the fluorescence intensity of the NV^- center, subtraction between these two images pixel by pixel effectively removed the background autofluorescence signals and significantly improved the image contrast. Although the protocol has been shown to be applicable to a number of biological systems ranging from single cells (such as HeLa cells) to small organisms (such as *C. elegans* and mice), post-processing data analysis is required. Hegyi and Yablonovitch[13] have similarly applied the optically detected magnetic resonance technique to image FNDs in tissue at the field-free region using an amplitude-modulated microwave source and a lock-in amplifier. The authors swept the field-free point across multiple FND targets within pieces of chicken breast and recorded the

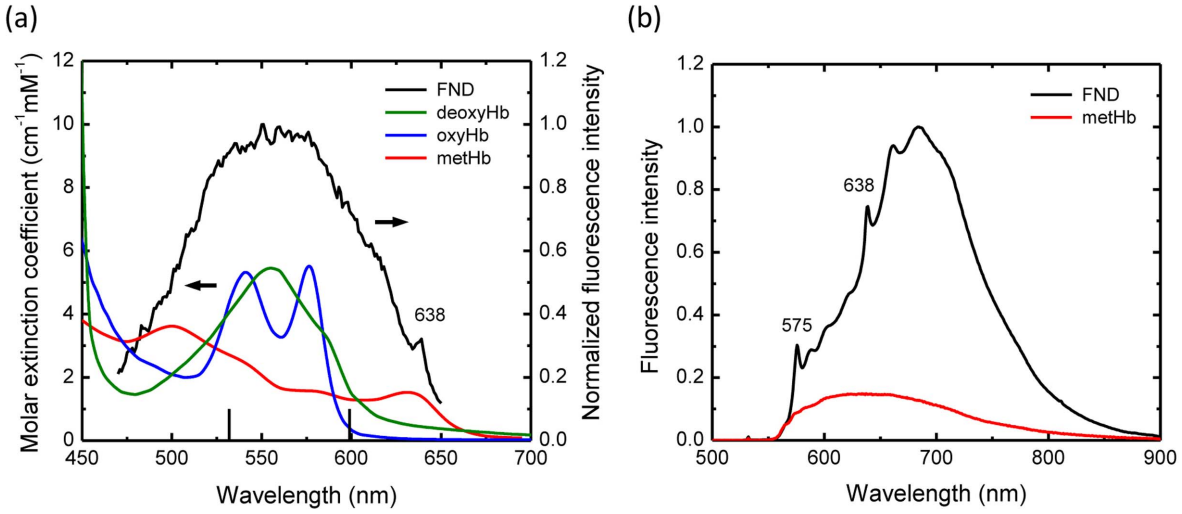

Figure 1 | Spectroscopic characterization of hemoglobin and fluorescent nanodiamond. (a) Comparison between the excitation spectrum of 100-nm FND and the absorption spectra of hemoglobin (Hb) in three different forms, deoxyHb, oxyHb, and metHb. The emission of FND was collected at 700–800 nm to obtain its excitation spectrum. Two vertical black lines indicate the points of the excitation at 532 nm and 599 nm. (b) Comparison between the fluorescence spectra of FND (1 mg/mL) and metHb (150 mg/mL) excited at 532 nm in water.

fluorescence intensity change correlated with FND distribution. A spatial resolution of ~800 μm was achieved. Most recently, Sarkar *et al.*[14] demonstrated a way of contrast enhancement for FNDs *in vivo* using a modulated external magnetic field. The field mixed the spin levels at the ground state, resulting in intensity modulation of the FND fluorescence, but not the background fluorescence[15]. The selective magnetic modulation technique improved the signal-to-background ratio by a factor of up to 100 and has been successfully applied for wide-field imaging of FNDs in sentinel lymph nodes of mice.

Here, we present an alternative approach to achieve background-free fluorescence imaging of FNDs both *in vitro* and *in vivo* by using an intensified charge-coupled device (ICCD) as the detector. ICCD is a high-sensitivity camera capable of high-speed gating operation to capture images of transient phenomena[16]. It is useful to suppress short-lifetime autofluorescence backgrounds and provide time-gated fluorescence images with high contrast. A number of efforts have been made in the past to employ high-cost, picosecond ICCD cameras for non-invasive *in vivo* imaging of biomolecules[17–19]. For FNDs which have a fluorescence lifetime of up to 20 ns, a nanosecond ICCD suffices. With this device and a Raman shifter, we have been able to obtain wide-field fluorescence images of single FND-labeled cancer cells free of tissue autofluorescence in whole blood and underneath a chicken breast of ~0.1 mm thickness. The wide-field fluorescence time gating technique has also allowed us to monitor the flow of FND-labeled cells in a microfluidic device and quantify the number of the cells in blood through flow cytometric analysis using an automatic cell counting program. An *in vivo* imaging application of this technique was demonstrated with FND-labeled lung cancer cells in the blood vessels of mouse ears. To the best of our knowledge, this is the first application of time-resolved CCD cameras for wide-field fluorescence imaging of FNDs and their labeled cells in living animals.

Results

Raman shifting. In biomedical imaging, it is well established that the major contribution of tissue absorption in the visible region is from hemoglobin (Hb). The molecule exhibits an intense Soret band at 409 nm, along with the *Q*-bands at around 550 nm, both arising from the π–π^* transitions of the heme groups[20]. Figure 1a shows the absorption spectra of Hb in three different forms (deoxyHb, oxyHb, and metHb) as well as the excitation spectrum of NV^- centers in FNDs over the wavelength range of 450–700 nm. The *Q*-bands of Hb substantially overlap with the absorption band peaking at ~560 nm associated with the ^3A–^3E transition of NV^{-12}. Upon exposure to green light at 532 nm, the Hb molecules emit broadband fluorescence over 550–750 nm, similar to that of the NV^- (Figure 1b). To reduce the level of the background fluorescence of Hb in blood, we performed Raman shifting of the green laser to the orange region, at which the absorption coefficient of the molecules drops by a factor of ~3 for Hb but remains about the same for NV^-. The orange light not only provides better image contrast for FND-labeled cells in blood but also penetrates deeper into tissue[21].

The experiment involved the use of a Q-switched, 1-ns, DPSS laser system with a repetition rate of 200 Hz and a total output power of 100 mW as the excitation source (cf. Figure 2a for the experimental setup). The choice of this laser system is a compromise between two requirements: 1) high repetition rate to match with the gating frequency (up to 50 kHz) of ICCD, and 2) high energy per pulse to achieve efficient stimulated Raman scattering (SRS). To perform SRS, the laser (1064 nm) was first frequency-doubled with a potassium titanyl phosphate (KTP) crystal and then red-shifted using a $Ba(NO_3)_2$ crystal (50 mm in length) as the Raman-active medium[22]. Figure 2b shows a chart recording the output laser energy of the second-order Stokes line at 599 nm versus the incident 532-nm laser energy. With the crystal orientation optimized for generating this Stokes component, a threshold of ~60 μJ and a conversion efficiency of 22% were obtained. The efficiency is about 4 times better than the previously reported for a Q-switched laser with a pulse width of 22 ps[23]. Moreover, the pulse width of the laser was reduced from 1.5 ns (532 nm) to 0.7 ns (599 nm) after SRS (Figure 2c). Such a line narrowing effect is in agreement with the observation for a 150-ps Nd:YAG laser at 1064 nm[24]. The pulse width of 0.7 ns is sufficiently small for the present time-gating measurement.

Fluorescence imaging. To verify the ability of our imaging system (Figure 2a), we have conducted a series of *in vitro* and *ex vivo* imaging experiments for FND-labeled cells. In the *in vitro* analysis, HeLa cells were first labeled with FNDs by endocytosis[25], as detailed in the experimental section. The FND-labeled cells were then immersed in human blood, sandwiched in between two glass slides, mounted on an upright microscope, and imaged by illumination with the 599-nm laser. Figure 3a and 3b compare fluorescence images of the FND-labeled HeLa cells without and with the time gating. The image contrast, defined by the ratio between the FND and background

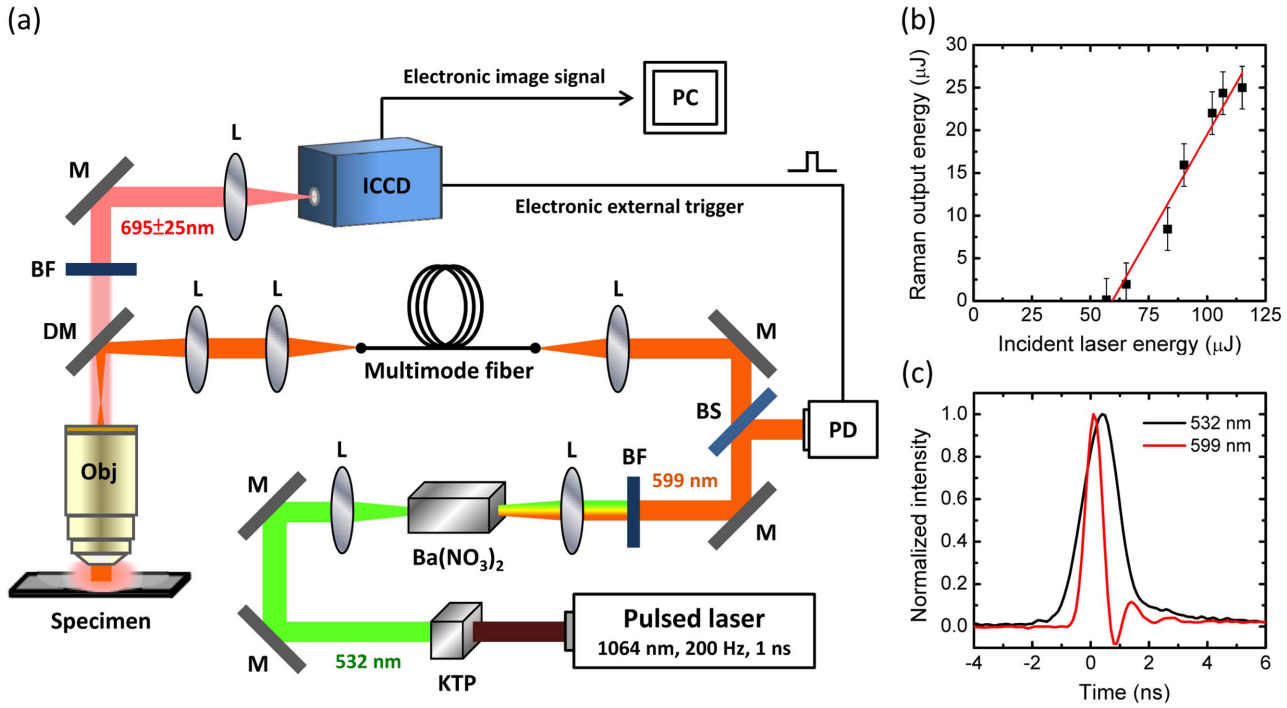

Figure 2 | The experimental setup. (a) Schematic of the wide-field time-gated fluorescence microscope. BF: bandpass filter, BS: beam splitter, DM: dichroic mirror, ICCD: intensified charge-coupled device, L: lens, M: mirror, Obj: objective, PC: personal computer, and PD: photodiode. The drawing was created with Microsoft Office PowerPoint 2007. (b) Power dependence of the second-order Stokes Raman conversion of the 532-nm laser using a $Ba(NO_3)_2$ crystal as the Raman shifter. The maximum output energy is about 25 μJ/pulse. (c) Oscilloscope traces of the laser pulses before and after passing through the Raman shifter.

fluorescence signals, is poor in Figure 3a because the Hb in blood (typically 150 mg/mL[26]) also emits strong red fluorescence upon excitation with the orange light. It is noted that the lifetime of the Hb fluorescence is in the range of 0.2 ns[27], which is much shorter than that of FND. The background noise can thus be effectively removed by setting the ICCD shutter time to be 10 ns. An improvement of the image contrast by a factor of ~20 was readily achieved when the time gating function was in use. The lateral resolution of the fluorescence imaging performed by using a 100× microscope objective is ~0.5 μm.

Next, to demonstrate the capability of the time-gating technique for potential *in vivo* imaging, we covered the FND-labeled HeLa cell sample in blood with a chicken breast of ~0.1 mm in thickness to simulate *in vivo* environment. Figure 4a presents a fluorescence image of the cells without time gating using a 40× microscope objective with a numerical aperture (NA) of 0.6. The image contrast is poor, with an average of ~2. Again, the time-gating technique can effectively improve the image contrast (Figure 4b). Referring to the data taken without chicken breast (Figure 4c), a deterioration of the lateral resolution from ~1 μm to ~5 μm due to light scattering by the tissue was found (Figure 4d). As the typical thickness of a mouse ear is 0.30 mm (or a skin thickness of less than 0.15 mm)[28], the result strongly suggests that our system is capable of imaging FND-labeled cells in the ear blood vessels of this animal model at the single cell level.

Flow cytometry. A 50-μm wide and 50-μm deep microchannel was employed for flow cytometric analysis of FND-labeled cells in human blood. The dimensions of the channel were chosen to resemble capillaries in mice and rats. We optically excited the sample with the 599-nm light and recorded the flow of the cells along the microchannel using our time-gated imaging system. The optimal frame rate of the recording was 23 Hz (or 43.5 ms/frame), with sequential readout of 34 × 514 pixels from the ICCD camera. Figure 5a displays snapshots of an FND-labeled cell flowing in the microchannel with human blood. With the syringe pump rate set at 0.1 mL/h, the speed of the flowing cell was estimated to be about 1 mm/s, which is close to the capillary blood flow rates of mice[29]. Direct measurement of the speed based on the size of the bright spots in the images showed an average of 0.56 mm/s for this particular cell in Figure 5a.

Next, we carried out flow cytometric analysis for a large number of cells to obtain a statistical sampling for the FND labeling performance. To facilitate the data analysis, we have developed a MATLAB program to count the cell number as well as to measure the fluorescence intensity of the FND-labeled cells flowing across the microchannel (see Supplementary Information for details). The program is so written that it counts only bright spots appearing in consecutive video frames as FND-labeled cells, while eliminating smaller spots that are most likely associated with noises (Supplementary Figure S1 and S2). A total of 862 FND-labeled cells flowing across the microchannel in 2200 s were detected and their fluorescence intensities were recorded accordingly. At the flow rate of 0.01 mL/h, the measured value matched well with the expected value of 998 cells. Figure 5b shows a histogram of the FND-labeled cells with different fluorescence intensities, i.e. different degrees of cellular uptake. The fluorescence intensity histogram closely resembles those provided by conventional flow cytometry, except that it has no (or little) background. The background-free nature of the time-gating technique makes it possible to recover rare events in high-background biological samples[30] and/or to differentiate cell types expressing low levels of surface antigens[31].

Moreover, we determined the efficiency of finding FND-labeled cells flowing across the microchannel as a function of the pumping rate using our imaging system. Table 1 summarizes the results obtained at different cell concentrations and cell flowing speeds at a frame rate of 23 Hz in 60 s. At the pumping rate below 0.05 mL/h, the measured and expected numbers of cells passing through the

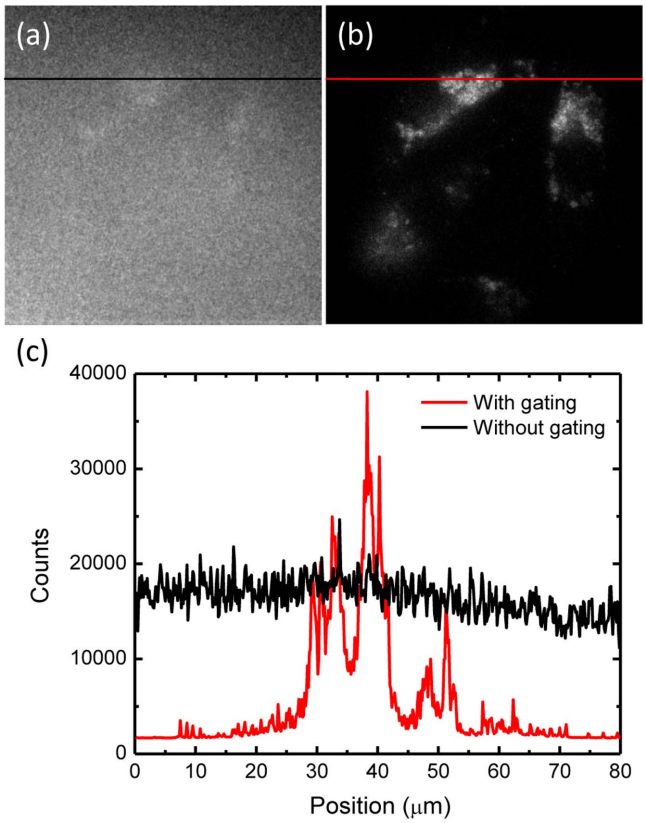

Figure 3 | *In vitro* imaging of FND-labeled cells in blood. (a, b) Wide-field fluorescence images of FND-labeled HeLa cells attached to a coverglass slide and immersed in human blood without (a) or with (b) time gating. The exposure times used for the fluorescence imaging with a 100× oil-immersion objective lens in (a) and (b) are 0.1 s and 0.3 s, respectively. (c) Intensity profiles along the black and red color lines denoted in (a) and (b), respectively.

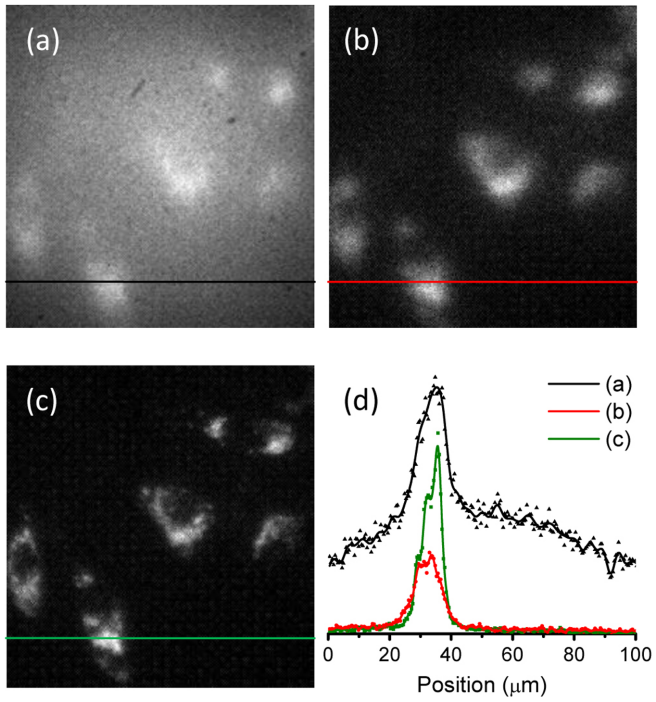

Figure 4 | *In vitro* imaging of FND-labeled cells covered with chicken breast. (a, b) Wide-field fluorescence images of FND-labeled HeLa cells in blood on a glass slide covered with a thin layer (~0.1 mm thickness) of chicken breast (a) without and (b) with time gating. (c) Time-gated fluorescence images of the corresponding FND-labeled HeLa cells in (a) and (b) without chicken breast. The objective lens is 40×. (d) Intensity profiles along the black, red color, and green lines denoted in (a), (b), and (c), respectively.

channel are close to each other, even at the concentration as low as 8300 cells/mL. However, as the pumping rate goes higher, the measured number of the FND-fed cells significantly deviates from the expected one because our system fails to identify fast-moving cells. The ability to detect FND-labeled HeLa cells at such a low concentration (8300 cells/mL or less) implies that the time-gated flow cytometric technique is applicable for tracking circulating tumor cells in blood without prior separation of red blood cells (RBCs)[32].

Finally, to prove the principle that our wide-field imaging system may serve as a useful instrument for *in vivo* flow cytometry[33,34], we labeled mouse lung cancer cells with FNDs and then injected them (1×10^5 cells in 100 μL) into a mouse via its tail vein. Fluorescence imaging was then carried out near one of the main blood vessels of the mouse ear. Shown in Figure 6a and 6b are bright-field and time-gated fluorescence images of the ear tissue. Much fluorescence background was detected even when the time gating function was switched on. The intense fluorescence signals arise predominantly from tissues such as the sebaceous glands upon excitation by the 599-nm light. They (as well as the residual fluorescence from the blood) are stationary and can be readily removed by background subtraction frame by frame. About 10 min after intravenous injection of the FND-labeled lung cancer cells into the mouse, bright moving objects with an average speed of 0.4 μm/s were clearly identified in the blood vessel at a frame rate of 2 Hz (Figure 6c). This measured speed is much lower than the blood flow velocity by ~3 orders of magnitude and thus most likely associated with rolling[35], instead of flowing, of the FND-labeled cells in the blood vessel.

Discussion

Wide-field imaging is a technique commonly used for *in vivo* imaging of small animals. The technique, however, often suffers from background noise problems due to cell and tissue autofluorescence. Subtraction between two images acquired at different wavelengths, either resonant or off-resonant with the absorption bands of the fluorescent markers, has been shown to be feasible to reduce the background level[36,37]. However, as the molecular imaging moves towards lower detection limits, a more effective method to eliminate background noises associated with the endogenous fluorescence *in vivo* is required. Among various fluorescence imaging instruments presently developed[38], the time-gating with time-correlated single photon counting (TCSPC) is an appealing approach. Although TCSPC-based pre-clinical optical imaging systems are now commercially available and have been applied to visualize fluorescent nanoparticles in small animals[39,40], their spatial resolution is limited to about 1 mm.

This work demonstrates a way of achieving a lateral resolution of better than 0.5 μm for FND-labeled cells in whole blood by wide-field time-gated fluorescence imaging as well as a resolution of ~5 μm when the cell sample is covered with a thin layer (~0.1 mm) of chicken breast to mimic *in vivo* environment. While the images have been severely blurred by tissue light scattering, single cell resolution is still achievable. Further improvement of the image contrast is plausible by using FNDs with higher fluorescence brightness and lasers with higher repetition rates and output powers. For instance, the image contrast could be greatly improved by use of a sub-nanosecond laser with a repetition rate of 50 kHz and a pulse energy of >20 μJ, although such lasers currently are not yet commercially available. However, in view of the rapid advancement in laser technology, together with the implementation of selective magnetic modulation[14],

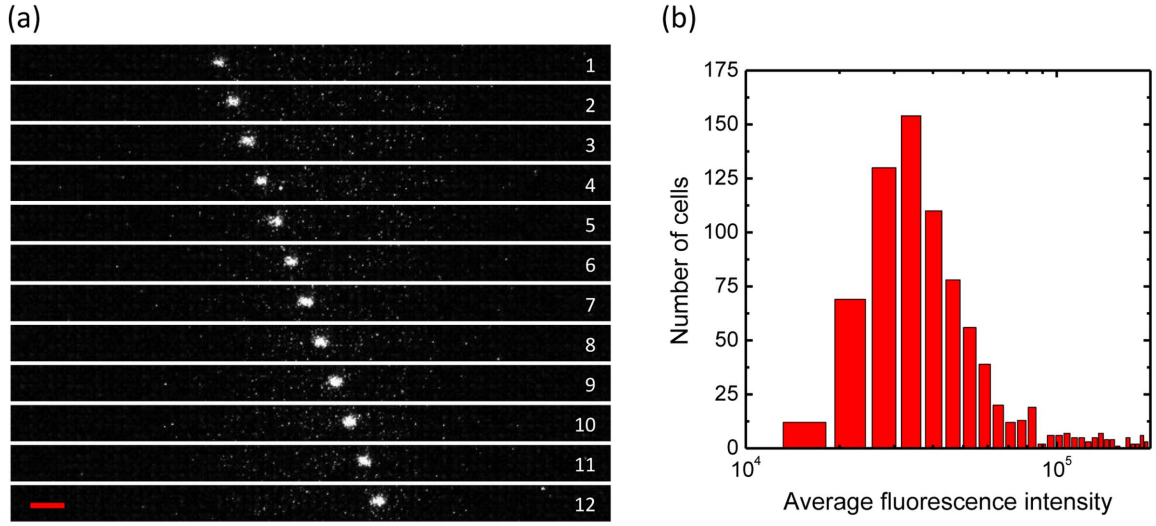

Figure 5 | Flow cytometric analysis of FND-labeled cells in a microchannel. (a) Snapshots of the flow of a single HeLa cell labeled with 100-nm FNDs in a microchannel with human blood. The channel width is 50 μm, the frame rate is 23 Hz (i.e. 43.5 ms/frame), and the objective lens is 10×. The red scale bar corresponds to 50 μm. (b) Histogram of the FND-labeled cells flowing across the microchannel with a cell concentration of 1.7×10^5 cells/mL and a pumping rate of 0.01 mL/h for 2155 s. The expected and counted numbers of the cells are 998 and 862, respectively.

we expect that the nanosecond wide-field time-gated imaging system will become a useful tool for long-term tracking and imaging of FND-labeled cancer cells near the skin surface of a mouse (with a typical skin thickness of ~0.5 mm) at the single cell level in coming years.

Flow cytometry is a powerful and versatile technique for quantifying multiple parameters of cells, including their morphology, functional state, proliferation, composition, and protein expression, etc. In conventional approaches of analyzing cells isolated from organs and tissues of mice or other animals, RBCs are first lysed and then the cells of interest (such as stem cells[41]) are extracted from the samples by either centrifugation or fluorescence-activated cell sorting. Using the experimental setup as illustrated schematically in Figure 2a, we show that it is possible to perform flow cytometric analysis of live cells without prior separation or lysis of RBCs. This is accomplished by labeling cells with FNDs and then analyzing them in whole blood using our homemade wide-field time-gated flow cytometer. The time-gating effectively suppresses background fluorescence signals, greatly enhances the visibility of FNDs, and has enabled us to detect the flow of FND-labeled HeLa cells in human blood at a concentration of lower than 8,000 cells/mL in capillary-sized microchannels.

Aside from the *in vitro* flow cytometric analysis, we have also shown that this wide-field time-gated imaging technique is capable of detecting FND-labeled cancer cells rolling in the blood vessels of a mouse ear with decent image contrast. Thanks to the FND's excellent photostability, we can track the movement of these cells in the bloodstream over a long period of time at the single cell level. The technique is promising for real-time imaging and tracking of transplanted stem cells in tissue repair and regeneration *in vivo*[41–43]. It can be applied for real-time tracking of FND-labeled cancer cells during metastasis *in vivo* as well.

As a final remark, we note that the presently developed technique is also potentially applicable for imaging free FNDs in the bloodstream of a living animal. Interesting questions such as how the FND particles escape from the labeled cells after cell death can be addressed. These particles are expected to accumulate in livers and spleens of the treated animals after release from the transplanted cells or following direct intravenous administration[44]. With FNDs properly conjugated with bioactive ligands or grafted with high-specificity antibodies against tumor-specific biomarkers (such as EpCAM[32]) through biotin-avidin interactions[45], *in vivo* imaging of circulating tumor cells in blood is deemed feasible in the near future.

Table 1 | Comparison between expected and counted numbers of FND-labeled HeLa cells passing through a microchannel at different cell concentrations and flow rates in human blood for 60 s

Cell concentration (10^4 cells/mL)	Pumping rate (mL/h)	Expected number	Counted number
0.83	0.02	3	4
0.83	0.05	7	8
0.83	0.10	14	1
17	0.01	28	24
17	0.10	280	40
33	0.01	55	65
170	0.01	280	248

Methods

Materials and chemicals. FNDs with size in the range of 100 nm were prepared as previously described using He^+ irradiation and subsequent annealing and air oxidation treatments[46]. Fresh human blood was donated by healthy adult volunteers at Academia Sinica, with informed consent from the participants. Cell culture medium and phosphate-buffered saline (PBS) were obtained from Biological Industries (USA). Hemoglobin and all other chemicals were purchased from Sigma-Aldrich (USA) and used without further purification.

Spectroscopic characterization. Excitation spectra of FNDs were acquired by using an inverted confocal microscope (Leica, SP8) equipped with a white-light continuum laser. To obtain the spectra, a FND sample was first prepared with a droplet of FND suspension placed on a coverglass slide and dried in air. The excitation wavelength of the continuum laser was then tuned from 470 nm to 670 nm with a prism, while the spectral window of the detector was fixed between 700 nm and 800 nm. Emission spectra of FNDs were acquired by using a setup built in-house for the particles suspended in water[46]. The spectrometer consisted of a 532-nm laser (Photop Suwtech, DPGL-2100F), a dichroic beam splitter (Chroma, Z532RDC), a long-working distance microscope objective (Mitutoyo, 50×, NA 0.55), a long-pass edge filter (Chroma, E550LP), and a multichannel analyzer (Hamamatsu, C7473). Backward fluorescence was collected to avoid strong light scattering loss and spectral distortion. The same setup was used to acquire the fluorescence spectra of human blood.

Cell culture and FND labeling. HeLa cells and mice lung cancer cells were cultured and labeled according to previous procedures[25]. Briefly, cells were maintained in regular Dulbecco's modified Eagle's medium (DMEM) supplemented with 10% fetal bovine serum and new born calf serum at 37°C in a humidified incubator with 5% CO_2. Before FND labeling, the cells were seeded at a density of 3×10^6 cells per 10-cm dish in culture medium and incubated overnight for cell attachment. About 1 mL of the FND suspension (100 μg/mL), prepared with serum-free DMEM, was pipetted into the dish containing the cells. Cellular uptake of FNDs was facilitated by incubation of the cells at 37°C with 5% CO_2 for 4 h, after which they were thoroughly

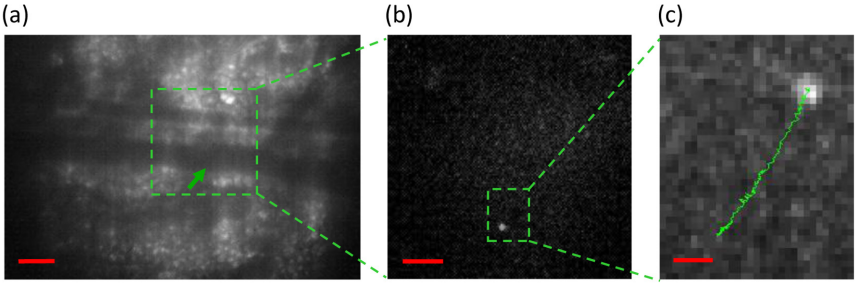

Figure 6 | *In vivo* imaging and tracking of FND-labeled cells in blood vessels. (a) Bright-field image of a mouse ear tissue. The green arrow indicates the position of an FND-labeled lung cancer cell in the blood vessel of ~50 μm in diameter. (b) Enlarged view of the fluorescence image of the square green region in (a). The bright spot corresponds to the FND-labeled lung cancer cell. (c) Enlarged view of the fluorescence image of the rectangular green region in (b), showing the trajectory of the FND-labeled lung cancer cell moving in the vessel. The average speed of the cell movement is 0.4 μm/s. The frame rate is 2 Hz and the objective lens is 10×. The red scale bar corresponds to 100, 50, and 10 μm in (a), (b) and (c), respectively.

washed with PBS to remove free FNDs and then harvested by trypsin treatment for subsequent analysis.

Experimental setup. The home-built fluorescence imaging and flow cytometry system (cf. Figure 2a) consisted of a SRS laser and an upright microscope (Nikon, Eclipse E600) equipped with an ICCD camera. To perform SRS, an infrared pulsed laser (Passat, Sub-Naples, 1064 nm, 200 Hz, 1 ns) was first frequency-doubled by a KTP crystal. The generated green light (532 nm) was then sent through a $Ba(NO_3)_2$ crystal (Molecular Technology, 10 mm × 10 mm × 50 mm), producing yellow and orange light. A bandpass filter (Semrock, FF01-600/14) isolated the second-order Stokes beam. Fluorescence imaging was conducted by splitting the 599-nm laser beam into two paths, one going to a photodiode (Thorlabs, DET10A) to provide a triggering signal for the ICCD (Andor, iStar DH712-18U-03) and the other one going to a 10-m optical fiber to delay the laser pulses to compensate for the gating time delay in ICCD. The latter laser beam was focused onto the sample through an objective lens and the resultant fluorescence was detected by the ICCD through an emission filter (670–720 nm). The average power of the laser after passing the microscope objective was ~4 mW (or ~20 μJ per laser pulse) and the field of view of the objective was 0.6 mm. The gating time of the ICCD was set at 10 ns throughout the entire experiment.

Flow cytometric analysis. Microchannels with dimensions of 50 μm in width and 50 μm in depth were obtained from Microfluidic Chip Shop (USA). A syringe pump (KD Scientific, KDS100) delivered the sample solution to the microchannel at a constant infusion rate of 0.01–1 mL/h. Flows of the FND-labeled cells in whole blood were recorded with our wide-field time-gated imaging system in video format, and the recorded videos were quantitatively analyzed by a MATLAB program. Details of the program developed specifically for quantifying the number of FND-labeled cells flowing along the microchannel are described in Supplementary Information. Briefly, the program was designed to take the place of human to quantify parameters such as brightness or speed for a large number of cells flowing through the microchannel. First, the video data, which were in the form of a series of matrices indicating the intensities of individual pixels, were fed to the MATLAB program to identify plausible bright spots as potential cell signals. Next, the program organized these spots in terms of location versus time (Supplementary Figure S2) and traced out straight lines through them. Since a flowing cell must appear in multiple frames in a linear fashion, only traceable spots were interpreted as a real cell signal. The program not only assigned traceable spots passing through the same straight lines as single cells, but also treated random photon bursts as background noises and removed them from the analysis. Afterwards, integrated fluorescence intensities of the individual cells were time-averaged and plotted in a histogram.

Animal experiment. BALB/C mice (weighing 25–30 g each) were purchased from the Animal Center of National Taiwan University Hospital. The animal to be studied was first anesthetized with intraperitoneal injection of avertin (composed of 2.5 g 2,2,2-tribromoethanol, 5 mL 2-methyl-2-butanol, and 200 mL H_2O). It was then placed on the stage of an upright microscope with one of its ears adhered to a microscope slide with glycerol (Supplementary Figure S3). FND-labeled cells in PBS were injected via the tail vein into the mouse at a concentration of 1×10^6 cells/mL and examined with the wide-field time-gated fluorescence imaging system (Figure 2a). During the entire study, the animals were maintained under specific pathogen-free conditions and were treated benevolently to eliminate or reduce suffering. The study was approved by the Institutional Animal Care and Use Committee of National Taiwan University (with IACUC Approval No: 20110331) and was conducted with compliance of standards established in the Guide for the Care and Use of Laboratory Animals[47].

1. Kircher, M. F., Gambhir, S. S. & Grimm, J. Noninvasive cell-tracking methods. *Nat. Rev. Clin. Oncol.* **8**, 677–688 (2011).
2. Baker, M. Nanotechnology imaging probes: Smaller and more stable. *Nat. Methods* **7**, 957–962 (2010).
3. Mochalin, V. N., Shenderova, O., Ho, D. & Gogotsi, Y. The properties and applications of nanodiamonds. *Nat. Nanotechnol.* **7**, 11–23 (2012).
4. Hui, Y. Y., Cheng, C.-L. & Chang, H.-C. Nanodiamonds for optical bioimaging. *J. Phys. D: Appl. Phys.* **43**, 374021 (2010).
5. Tisler, J. *et al.* Fluorescence and spin properties of defects in single digit nanodiamonds. *ACS Nano* **3**, 1959–1965 (2009).
6. Fu, C.-C. *et al.* Characterization and application of single fluorescent nanodiamonds as cellular biomarkers. *Proc. Natl. Acad. Sci. USA* **104**, 727–732 (2007).
7. Su, L.-J. *et al.* Creation of high density ensembles of nitrogen-vacancy centers in nitrogen-rich type Ib nanodiamonds. *Nanotechnology* **24**, 315702 (2013).
8. Billinton, N. & Knight, A. W. Seeing the wood through the trees: a review of techniques for distinguishing green fluorescent protein from endogenous autofluorescence. *Anal. Biochem.* **291**, 175–197 (2001).
9. Faklaris, O. *et al.* Detection of single photoluminescent diamond nanoparticles in cells and study of the internalization pathway. *Small* **4**, 2236–2239 (2008).
10. Kuo, Y., Hsu, T.-Y., Wu, Y.-C. & Chang, H.-C. Fluorescent nanodiamond as a probe for the intercellular transport of proteins *in vivo*. *Biomaterials* **34**, 8352–8360 (2013).
11. Igarashi, R. *et al.* Real-time background-free selective imaging of fluorescent nanodiamonds *in vivo*. *Nano Lett.* **12**, 5726–5732 (2012).
12. Jelezko, F. & Wrachtrup, J. Single defect centres in diamond: A review. *Phys. Status Solidi* **203**, 3207–3225 (2006).
13. Hegyi, A. & Yablonovitch, E. Molecular imaging by optically-detected electron spin resonance of nitrogen-vacancies in nanodiamond. *Nano Lett.* **13**, 1173–1178 (2013).
14. Sarkar, S. K. *et al.* Wide-field *in vivo* background free imaging by selective magnetic modulation of nanodiamond fluorescence. *Biomed. Opt. Express* **5**, 1190–1202 (2014).
15. Chapman, R. & Plakhotnik, T. Background-free imaging of luminescent nanodiamonds using external magnetic field for contrast enhancement. *Opt. Lett.* **38**, 1847–1849 (2013).
16. Fickler, R., Krenn, M., Lapkiewicz, R., Ramelow, S. & Zeilinger, A. Real-time imaging of quantum entanglement. *Sci. Rep.* **3**, 1914 (2013).
17. Sun, Y. *et al.* Fluorescence lifetime imaging microscopy: *in vivo* application to diagnosis of oral carcinoma. *Opt. Lett.* **34**, 2081–2083 (2009).
18. Venugopal, V., Chen, J. & Intes, X. Development of an optical imaging platform for functional imaging of small animals using wide-field excitation. *Biomed. Opt. Express* **1**, 143–156 (2010).
19. McGinty, J. *et al.* Wide-field fluorescence lifetime imaging of cancer. *Biomed. Opt. Express* **1**, 627–640 (2010).
20. Zijlstra, W. G., Buursma, A. & van Assendelft, O. W. *Visible and Near Infrared Absorption Spectra of Human and Animal Haemoglobin* (VSP, Utrecht, 2000).
21. Juzenas, P., Juzeniene, A., Kaalhus, O., Iani, V. & Moan, J. Noninvasive fluorescence excitation spectroscopy during application of 5-aminolevulinic acid *in vivo*. *Photochem. Photobiol. Sci.* **1**, 745–748 (2002).
22. Pask, H. M. The design and operation of solid-state Raman lasers. *Prog. Quantum Electron.* **27**, 3–56 (2003).
23. Zverev, P. G., Murray, J. T., Powell, R. C., Reeves, R. J. & Basiev, T. T. Stimulated Raman scattering of picosecond pulses in barium nitrate crystals. *Optics Commun.* **97**, 59–64 (1993).
24. Agnesi, A., Caracciolo, E., Carrà, L., Pirzio, F. & Reali, G. 150-ps pulse Raman generator pumped by a 1-kHz sub-nanosecond passively Q-switched laser system. *Appl. Phys. B* **107**, 691 (2012).
25. Fang, C.-Y. *et al.* The exocytosis of fluorescent nanodiamond and its use as a long-term cell tracker. *Small* **7**, 3363–3370 (2011).
26. Vajpayee, N., Graham, S. S. & Bem, S. [Basic examination of blood and bone marrow] *Henry's Clinical Diagnosis and Management by Laboratory Methods*

[McPherson, R. A. & Pincus, M. R. (eds.)] [509–535] (Saunders/Elsevier, Philadelphia, 2011).
27. Zheng, W., Li, D., Zeng, Y., Luo, Y. & Qu, J. Y. Two-photon excited hemoglobin fluorescence. *Biomed. Opt. Express* **2**, 71–79 (2011).
28. Thorne, P. S., Hawk, C., Kaliszewski, S. D. & Guiney, P. D. The noninvasive mouse ear swelling assay. I. Refinements for detecting weak contact sensitizers. *Fundam. Appl. Tox.* **17**, 790–806 (1991).
29. Chen, Z. *et al.* Noninvasive imaging of *in vivo* blood flow velocity using optical Doppler tomography. *Opt. Lett.* **22**, 1119–1121 (1997).
30. Jin, D. *et al.* Time-gated flow cytometry: an ultra-high selectivity method to recover ultra-rare-event μ-targets in high-background biosamples. *J. Biomed. Opt.* **14**, 024023 (2009).
31. Lu, J. *et al.* Resolving low-expression cell surface antigens by time-gated orthogonal scanning automated microscopy. *Anal. Chem.* **84**, 9674–9678 (2012).
32. Balic, M., Williams, A., Lin, H., Datar, R. & Cote, R. J. Circulating tumor cells: From bench to bedside. *Annu. Rev. Med.* **64**, 31–44 (2013).
33. Novak, J., Georgakoudi, I., Wei, X., Prossin, A. & Lin, C. P. *In vivo* flow cytometer for real-time detection and quantification of circulating cells. *Opt. Lett.* **29**, 77–79 (2004).
34. Nedosekin, D. A. *et al.* Synergy of photoacoustic and fluorescence flow cytometry of circulating cells with negative and positive contrasts. *J. Biophoton.* **6**, 425–434 (2013).
35. McEver, R. P. & Zhu, C. Rolling cell adhesion. *Annu. Rev. Cell Dev. Biol.* **26**, 363–396 (2010).
36. Troy, T., Jekic-McMullen, D., Sambucetti, L. & Rice, B. Quantitative comparison of the sensitivity of detection of fluorescent and bioluminescent reporters in animal models. *Mol. Imaging* **3**, 9–23 (2004).
37. Vaijayanthimala, V. *et al.* The long-term stability and biocompatibility of fluorescent nanodiamond as an *in vivo* contrast agent. *Biomaterials* **33**, 7794–7802 (2012).
38. Leblond, F., Davis, S. C., Valdes, P. A. & Pogue, B. W. Pre-clinical whole-body fluorescence imaging: Review of instruments, methods and applications. *J. Photochem. & Photobiol. B* **98**, 77–94 (2010).
39. Christian, N. A. *et al. In vivo* dendritic cell tracking using fluorescence lifetime imaging and near-infrared-emissive polymersomes. *Mol. Imaging Biol.* **11**, 167–177 (2009).
40. Gu, L. *et al. In vivo* time-gated fluorescence imaging with biodegradable luminescent porous silicon nanoparticles. *Nat. Commun.* **4**, 2326 (2013).
41. Wu, T.-J. *et al.* Tracking the engraftment and regenerative capabilities of transplanted lung stem cells using fluorescent nanodiamonds. *Nat. Nanotechnol.* **8**, 682–689 (2013).
42. Xu, C. *et al.* Tracking mesenchymal stem cells with iron oxide nanoparticle loaded poly(lactide-co-glycolide) microparticles. *Nano Lett.* **12**, 4131–4139 (2012).
43. Hsu, T.-C., Liu, K.-K., Chang, H.-C., Hwang, E. & Chao, J.-I. Labeling of neuronal differentiation and neuron cells with biocompatible fluorescent nanodiamonds. *Sci. Rep.* **4**, 5004 (2014).
44. Yuan, Y., Chen, Y., Liu, J.-H., Wang, H. & Liu, Y. Biodistribution and fate of nanodiamonds *in vivo*. *Diamond Relat. Mater.* **18**, 95–100 (2009).
45. Chang, B.-M. *et al.* Highly fluorescent nanodiamonds protein-functionalized for cell labeling and targeting. *Adv. Funct. Mater.* **23**, 5737–5745 (2013).
46. Chang, Y.-R. *et al.* Mass production and dynamic imaging of fluorescent nanodiamonds. *Nat. Nanotechnol.* **3**, 284–288 (2008).
47. Liu, C.-L. *et al. In vivo* metabolic imaging of insulin with multiphoton fluorescence of human insulin-Au nanodots. *Small* **9**, 2103–2110 (2013).

Acknowledgments

This work is supported by Academia Sinica and the National Science Council of Taiwan with Grant No. 102-2119-M-001-001-. We thank Yu-Fang Shen and Pei-Chun Wu for technical assistance in animal experiments.

Author contributions

Y.Y.H., L.-J.S. and O.Y.C. conducted experiments, Y.-T. Chen, T.-M. L. and H.-C.C. supplied materials and equipments, Y.Y.H., L.-J.S., O.Y.C. and H.-C.C. designed experiments and wrote the manuscript.

Additional information

Supplementary information accompanies this paper at http://www.nature.com/scientificreports

Competing financial interests: The authors declare no competing financial interests.

How to cite this article: Hui, Y.Y. *et al.* Wide-field imaging and flow cytometric analysis of cancer cells in blood by fluorescent nanodiamond labeling and time gating. *Sci. Rep.* **4**, 5574; DOI:10.1038/srep05574 (2014).